Growth kinetics and abrasive wear resistance of boride layers on Fe–15Cr alloy

V. I. Dybkov*, L. V. Goncharuk, V. G. Khoruzha, A. V. Samelyuk and V. R. Sidorko

Two boride layers based on the FeB and Fe_2B compounds are formed at the interface between an Fe–15Cr alloy and boron at 850–950°C and reaction times up to 12 h, with the average chromium content being around 8 at-% in the former and 12 at-% in the latter. Both boride layers reveal a pronounced texture. Diffusional growth kinetics of the layers are close to parabolic and can alternatively be described by a system of two non-linear differential equations. Microhardness values are 17·4 GPa for the FeB layer, 14·4 GPa for the Fe_2B layer and 0·95 GPa for the Fe–15Cr alloy base. The dry abrasive wear resistance of borided alloy samples is around 45 times greater than that of non-borided ones.

Keywords: Fe–15Cr alloy, Boron, Boride layers, Growth kinetics, Wear resistance

Introduction

Boriding is one of the thermochemical surface treatments often used to improve service characteristics (hardness, mechanical and corrosive wear resistance, etc.) of metals, alloys and steels.[1–24] Iron borides FeB and Fe_2B are known to exist in the Fe–B binary system.[25,26] With Fe, its alloys and steels, one (either FeB or Fe_2B) or two (both FeB and Fe_2B) boride layers can therefore form on the surface of a substrate, depending on boriding techniques employed and temperature–time conditions of a boriding procedure.

The properties of iron boride layers are, to a large extent, dependent on the amount of alloying elements and impurities present in a base material. In the case of materials of complicated chemical composition, for example steels or multicomponent alloys, it is not so easy to separate the effect of a particular element from that of others. Therefore, experiments with binary alloys are desirable. In the present work, the data on the interaction of a Fe–15Cr alloy with B in a mixture of amorphous B powder and KBF_4 at 850–950°C are presented, with the main emphasis on establishing the boride layer growth kinetics that received comparatively little attention. Furthermore, the results of dry abrasive wear resistance tests of boride layers are reported.

Experimental

Materials and specimens

The materials used included high purity Fe powder (99·98%Fe), electrolytic grade Cr platelets (99·98%Cr), amorphous B and analytical grade KBF_4. All contents are given in mass per cent if otherwise not stated.

Initially, the B powder contained 98·3%B, 0·04%C, 1·6%O and insignificant amounts of Si, Cu, Mg (<0·01% each) and Fe (<0·001%). Before the boriding experiments, the powder was first heated slowly in vacuum up to 1450°C and then calcined at this temperature for 2 h in an atmosphere of Ar at a pressure of $2{\cdot}5 \times 10^4$ Pa to remove volatile oxides. KBF_4 was preliminary dried in steps at 95, 110, 130 and 170°C (24 h at each temperature).

Cylindrical rods of a Fe–15Cr alloy were prepared by arc melting of appropriate metals under Ar, with subsequent casting of the melts into water cooled copper crucibles. The rods were annealed to ensure their homogenisation at a temperature of 1100°C for 2 h in an Ar atmosphere at a pressure of $2{\cdot}5 \times 10^4$ Pa.

Specimens in the form of tablets, 11·28 mm in diameter (1·0 cm^2 area) and 5·5 mm in height, were machined from the Fe–Cr alloy rods. Flat sides of the tablets were ground and polished mechanically.

Experimental methods

The vacuum device VPBD-2S employed for boriding Fe–Cr alloy samples has been described elsewhere.[27] Its experimental cell is shown in Fig. 1. The experiment was carried out in an alumina crucible, 13 mm inner diameter and 40 mm height.

A Fe–Cr alloy tablet was embedded into a mixture of B powder with 5%KBF_4 as an activator. This amount of KBF_4 is considered to be optimum.[1,28] The mixture was then slightly pressed, and a load of 8·5 g (a low C steel cylinder) was placed on top. The crucible was closed with a low C steel lid and placed into a steel sheet holder, mounted to a guide rod capable of moving in the vertical direction.

The chamber was pumped to a pressure of ~10 Pa and filled with high purity Ar (99·999 vol.-%Ar). This

Department of Physical Chemistry of Inorganic Materials, Institute for Problems of Materials Science, Kyiv 03180, Ukraine

*Corresponding author, email vdybkov@ukr.net

© 2011 Institute of Materials, Minerals and Mining
Published by Maney on behalf of the Institute
Received 21 January 2010; accepted 4 February 2010
DOI 10.1179/026708310X12683157551577

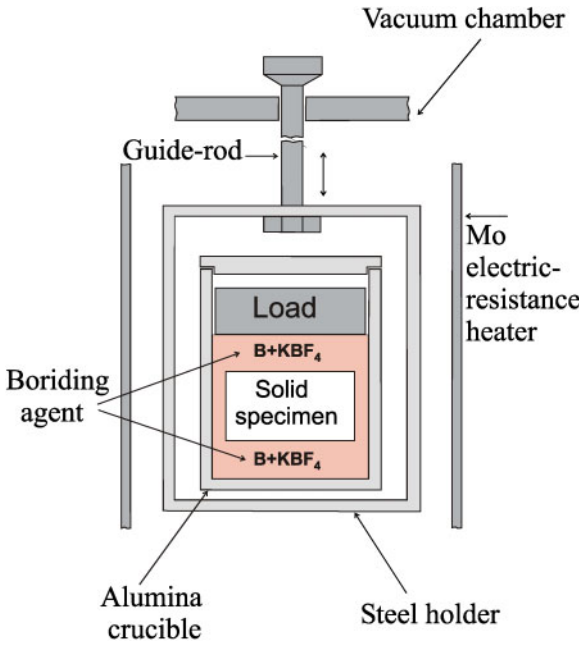

1 Experimental cell

procedure was repeated twice. Then, the chamber was again pumped and filled with Ar at a pressure of $2{\cdot}5 \times 10^4$ Pa, and heating was started. During heating, the crucible with its contents was in the cold zone above the furnace. After the required temperature in the range of 850–950°C had been reached in the furnace, the crucible, preheated to ~400°C, was moved into its middle part. After an initial drop, the temperature attained its predetermined value in 4–5 min and was then maintained constant within ± 1°C with the help of an automatic thermoregulator VRT-3. The temperature measurements were carried out using a Pt–PtRh thermocouple. The experiments were carried out at temperatures of 850, 900 and 950°C. Their duration was 3600–43 200 s (1–12 h).

After the experiment, the tablet with boride layers was cut along the cylindrical axis into two unequal parts (4 and 7 mm) using an electric spark machine. Its greater part was embedded into a cold setting epoxy resin and used to prepare a metallographic cross-section. The lesser part was used for X-ray diffraction investigations (plan view samples).

Characterisation of initial materials and boride layers was carried out with the help of metallography, X-ray and chemical analyses and electron probe microanalysis (EPMA). The thickness of boride layers was evaluated using the pictures obtained on an optical microscope MIM-7 equipped with an HP Photosmart 720 camera. Typically, six pictures were taken at different places of the interface ($\sim$1 cm long on any cross-section) between the reacting phases. The thickness of each boride layer was calculated by dividing the area occupied by that layer by the length of a region under examination, and the average value of six measurements was found. The mean relative error of determination of the layer thickness was estimated to be around $\pm 12\%$.

The chemical composition of the layers and the concentration profiles of the elements in the transition zone between reacting phases were obtained using an electron probe microanalyser JEOL Superprobe 733. The beam spot diameter and the phase volume analysed at each point were estimated to be about 1 and 2 μm^3 respectively.

X-ray diffraction patterns were taken immediately from the surface of tablet samples on a DRON-3 apparatus using Cu K_α radiation. When taking the first pattern, no polishing of a borided sample was applied (section 0). Then, 10 μm of a boride layer was removed by grinding and subsequent polishing, and another X-ray diffraction pattern was taken (section I). This procedure was repeated at a step of 30–50 μm until the base material was reached (sections II–VII). Eight X-ray diffraction patterns were thus taken on each borided sample.

Microhardness measurements on metallographic cross-sections were carried out using a standard PMT-3 tester with the diamond pyramid (Vickers indenter). The load was 0·98 N (100 g).

Abrasive wear resistance tests (each along a fresh track) were carried out on P180 SiC emery paper tape (main fraction grain size, 63 μm; maximum, 90 μm) using an AWRD-5 device.[29] The velocity of continuous movement of the tape (25·0 m long) was 0·35 m s^{-1}, while the gauge length during each test was 22·0 m. The load was 50 N (5·1 kg). The wear resistance was determined by means of weighing the samples and measuring their height.

Phase identity and chemical composition of boride layers

Two boride phases were found to form as separate layers at the alloy/B interface at 850–950°C and reaction times up to 12 h (Fig. 2). Plan view layer by layer X-ray analysis of borided samples (Fig. 3) and a further comparison of our study and literature[30–35] data showed the outer layer bordering the boriding agent to be the FeB phase while the inner layer adjacent to the alloy base to be the Fe_2B phase (Fig. 4). The two phase zone near the continuous Fe_2B layer consists of the Fe_2B (and occasionally Cr_2B) phase and the alloy base of somewhat different composition compared to the nominal one.

As seen from cross-sectional micrographs in Figs. 2 and 3, both layers consist of columnar crystals oriented preferentially in the direction of diffusion. Their characteristic feature is a tooth-like morphology and pronounced texture. This is considered to be a consequence of the existence of paths of enhanced diffusion in the crystal lattices of FeB and Fe_2B.[1,18] If such paths are not available (close rates of diffusion in all crystallographic directions), flat boride layers are formed (see, for example, Ref. 28).

The strongest reflections are {002} ($2\theta = 63{\cdot}07°$ and spacing $d = 0{\cdot}1474$ nm) and, to a lesser extent, {020} ($2\theta = 32{\cdot}63°$ and $d = 0{\cdot}2744$ nm) for the orthorhombic FeB phase, and {002} ($2\theta = 42{\cdot}55°$ and $d = 0{\cdot}2125$ nm) for the tetragonal Fe_2B phase. The change in intensities of those reflections with increasing distance from the surface of a borided alloy tablet is illustrated in Fig. 5. Numerical values of intensities are presented in Table 1. It should be noted that with isotropic microcrystalline samples, the strongest reflections are {111}, {200} and {210} for FeB and {211} for Fe_2B.[30–33]

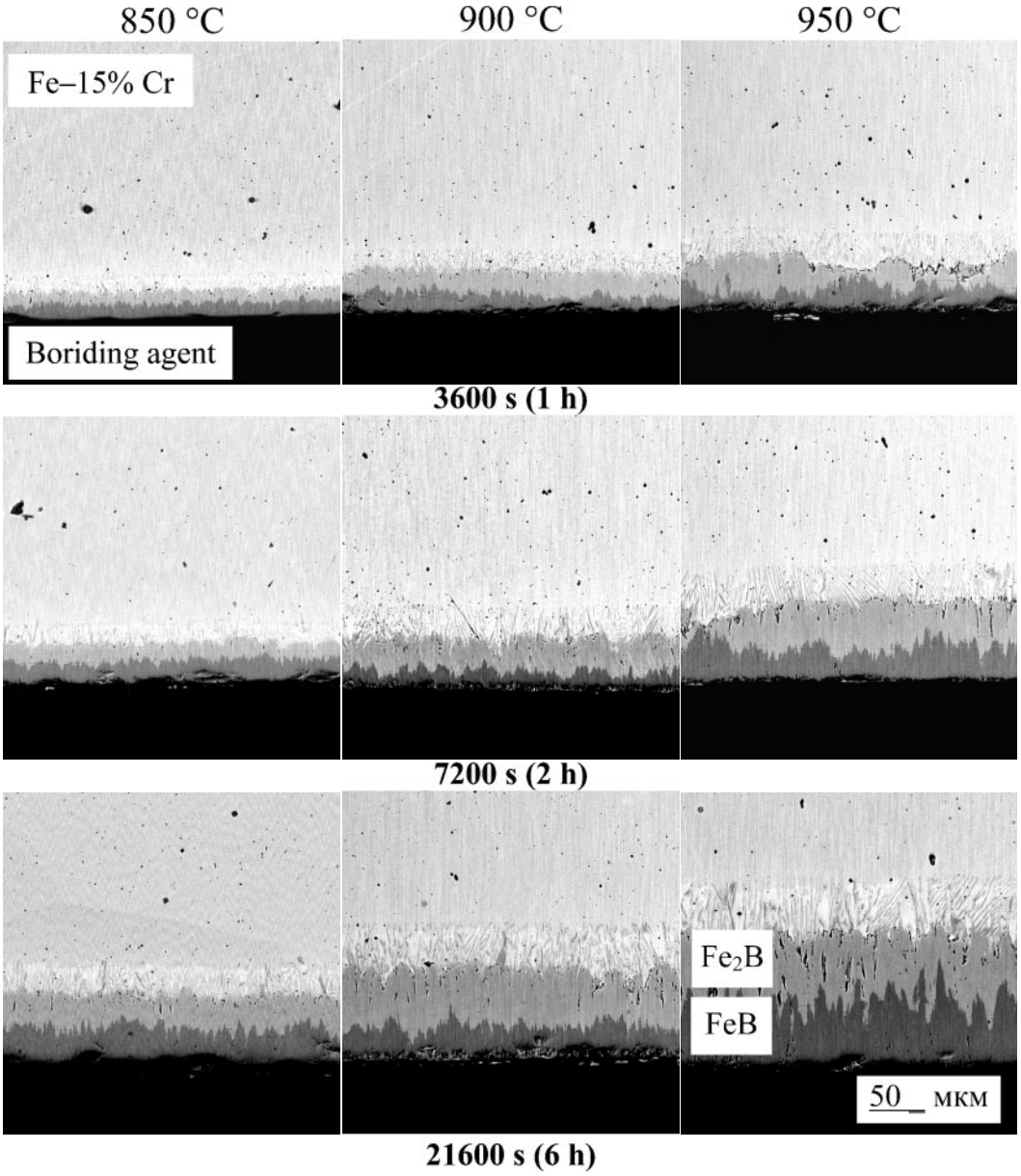

2 Backscattered electron images of Fe–15Cr alloy/B interface. Darker layer bordering boriding agent is FeB phase, while brighter layer adjacent to alloy base is Fe_2B phase. Two phase zone near Fe_2B layer consists of Fe_2B (and occasionally Cr_2B) phases and alloy matrix

As evidenced from Table 1, the larger orientation order is characteristic of the inner portions of both boride layers compared to their near interface portions, in agreement with findings of other researchers.[1,13,18] This is easily explainable because near interface portions of any boride layer are less equilibrated compared to its inner portions. Therefore, near interface crystals have less time to align in the preferred direction.

X-ray investigations were followed by EPMA measurements. As seen in Fig. 3, sections 0 and I of a borided Fe–15Cr sample corresponded to the FeB phase. Average Fe, Cr and B contents of this and other phases, found by EPMA measurements on X-ray diffraction samples, are provided in Table 2. Sections II and III crossed both the FeB and Fe_2B phases (Figs. 3 and 6), with the FeB phase dominating in section II and the Fe_2B phase prevailing in section III. Section IV only corresponded to the Fe_2B phase. The microstructure of sections V (Fig. 7) and VI (Fig. 8) consisted of Fe_2B with rare inclusions of Cr_2B and the alloy base depleted in Cr compared to the nominal one, while that of section VII was entirely the alloy base of nominal composition 85Fe–15Cr.

Electron probe microanalysis measurements across the reacting phases (Table 3) did not reveal any noticeable homogeneity ranges of the FeB and Fe_2B phases. Both phases dissolve considerable amounts of Cr, and therefore, their chemical formulae should be expressed as (Fe,Cr)B and $(Fe,Cr)_2B$ respectively. Simplified designations FeB and Fe_2B are only used for brevity.

The distribution of Cr within the boride layers is rather irregular (Fig. 9) due probably to non-equilibrium conditions of layer formation. The Cr content is 8 ± 1 at-% in the (Fe,Cr)B layer and 12 ± 2 at-% in the $(Fe,Cr)_2B$ layer. These values agree fairly well with the literature.[13,36]

Microhardness of boride phases

Microhardness of the FeB layer was found to be $17{\cdot}4 \pm 0{\cdot}9$ GPa while that of the Fe_2B layer was

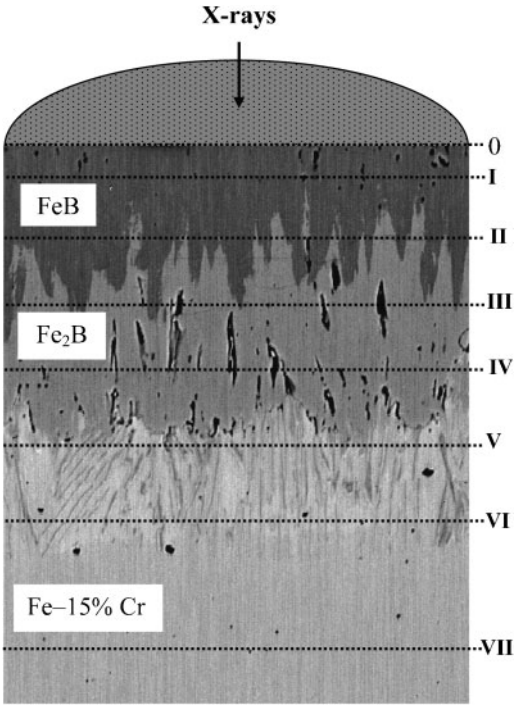

3 Scheme of X-ray diffraction investigations of borided Fe–15Cr alloy sample: boriding conditions, 950°C and 21 600 s (6 h); distance between successive sections of sample (from top deeper inside its bulk), 10 μm (0–I), 30 μm (I–II), 30 μm (II–III), 30 μm (III–IV), 30 μm (IV–V), 30 μm (V–VI) and 50 μm (VI–VII)

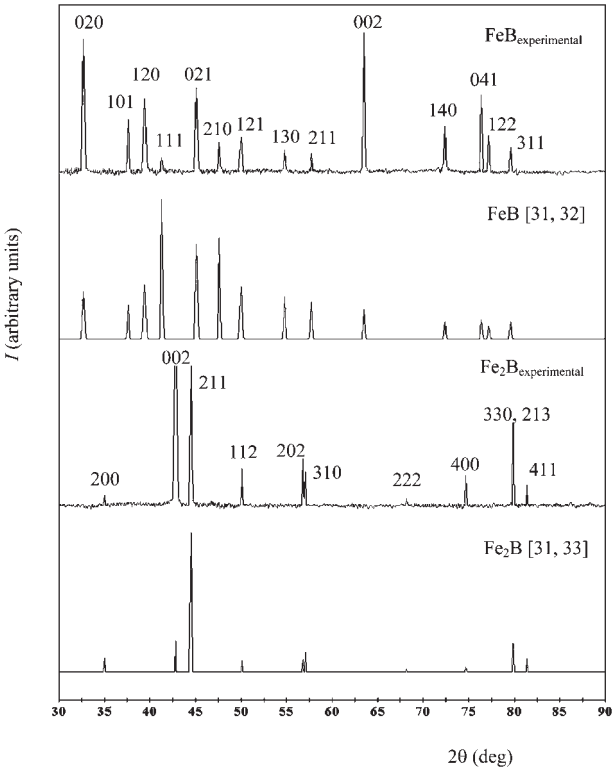

4 Comparison of our experimental and literature[31–33] X-ray diffraction patterns of FeB and Fe_2B phases formed at Fe–15Cr alloy/B interface after boriding at temperature of 950°C for 21 600 s (6 h): experimental pattern of FeB phase was taken from section 0, while that of Fe_2B phase was taken from section IV (see Fig. 3)

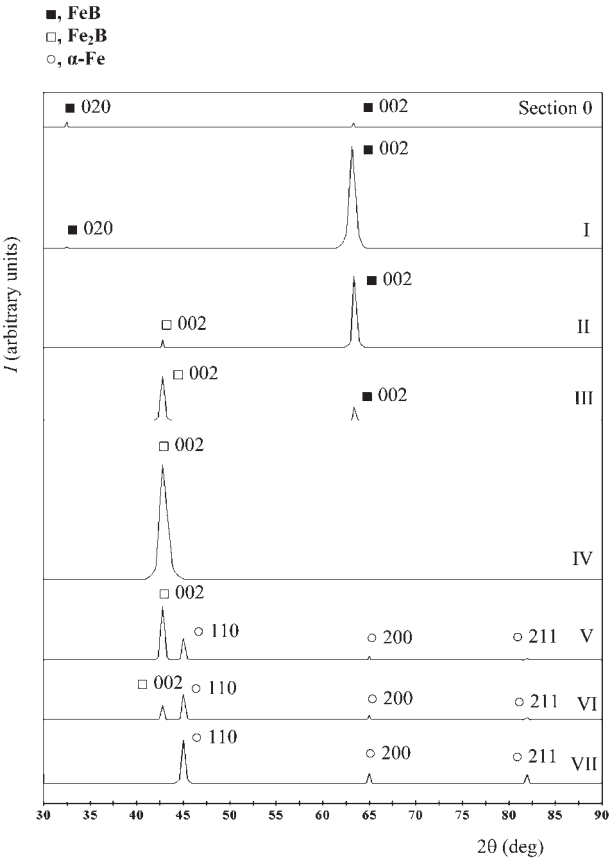

5 Most intensive peaks of X-ray diffraction patterns taken from different plan view sections of Fe–15Cr alloy sample borided at 950°C for 21 600 s (6 h) (see also Fig. 3 and Table 1): change in their intensity provides evidence for formation of texture of FeB and Fe_2B layers

$14{\cdot}4 \pm 0{\cdot}8$ GPa. For the Fe–15Cr alloy base, its value is $0{\cdot}95 \pm 0{\cdot}08$ GPa.

A plot of microhardness values against distance across the reacting phases is shown in Fig. 10. Microhardness is practically constant within both boride layers and the alloy base, except in the vicinity of the inner boride layer where it slightly diminishes (by ~0·2 GPa) with increasing distance in the range 0–200 μm.

Table 1 X-ray diffraction data showing preferential directions of growth for FeB and Fe_2B phases formed at interface between Fe–15Cr alloy and B after boriding at temperature of 950°C for 21 600 s (6 h) (see also Fig. 5)

			Peak intensity (arbitrary units)							
Phase	*hkl*	*d*, nm	0*	I	II	III	IV	V	VI	VII
FeB	020	0·275	150	17	9					
	002	0·148	128	2500	1750	332				
Fe_2B	002	0·212			215	1080	2800	1300	350	
α-Fe	110	0·201						538	625	1050
	200	0·143						103	120	250
	211	0·117						42	55	219

*Serial numbers of appropriate sections of a borided tablet sample by a plane parallel to its flat surface (section 0, I and so on, deeper into the sample bulk, see Fig. 3).

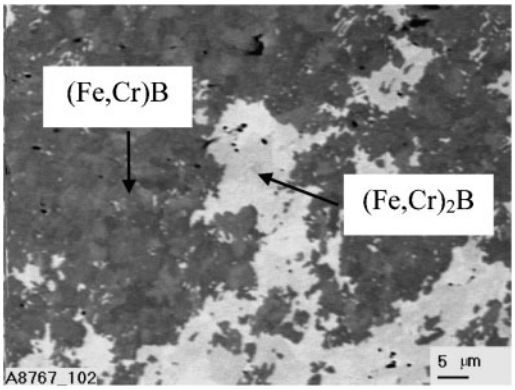

6 Plan view micrograph corresponding to section II in Fig. 3

Layer growth kinetics

After the continuous layers of both borides have formed, their subsequent diffusional growth is due to two partial chemical reactions (Fig. 11)

$$B_{dif} + Fe_2B = 2FeB \quad (1a)$$

and

$$Fe_{dif} + FeB = Fe_2B \quad (1b)$$

The diffusional growth kinetics of compound layers are often treated using parabolic equations of the type $x^2=2k_1t$, where x is the layer thickness, k_1 is the layer growth rate constant and t is time.[37,38] For sufficiently thick layers, such equations produce a quite satisfactory fit to the experimental data (Fig. 12 and Table 4). In view of a relatively large experimental error in the determination of layer thicknesses, acceptable results are also obtained for the total thickness of both layers, even though the sum of any two parabolas is clearly not a parabola. Since such data are of interest for practical applications, they are included in Fig. 12 and Table 4 as well.

In fact, however, growth kinetics of the FeB and Fe_2B layers at the diffusional stage of their formation are somewhat more complicated and can alternatively be described by a system of two non-linear differential equations[39]

$$\frac{dx}{dt} = \frac{k_B}{x} - \frac{rg}{p}\frac{k_{Fe}}{y} \quad (2a)$$

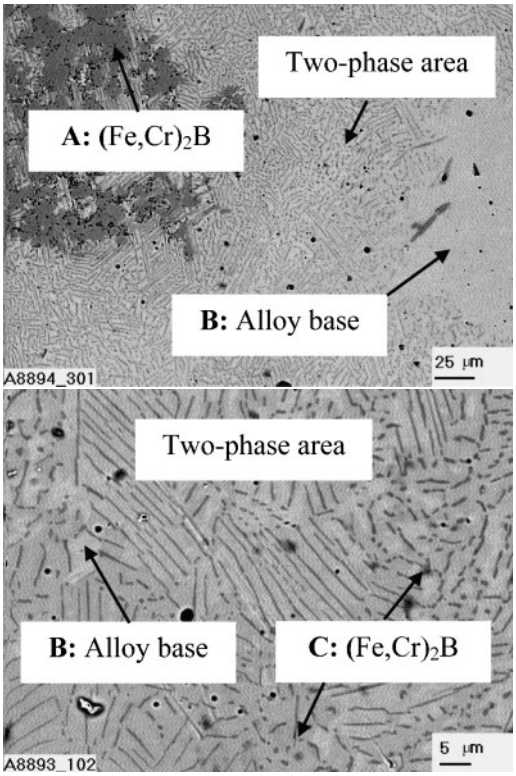

7 Plan view micrographs corresponding to section V in Fig. 3

$$\frac{dy}{dt} = \frac{k_{Fe}}{y} - \frac{q}{sg}\frac{k_B}{x} \quad (2b)$$

where x is the FeB layer thickness, y is the Fe_2B layer thickness, k_B is the FeB layer growth rate constant, k_{Fe} is the Fe_2B layer growth rate constant, g is the ratio of the molar volumes of the FeB and Fe_2B compounds, $p=q=r=1$ and $s=2$ (factors from the chemical formulae of FeB and Fe_2B).

Under conditions of diffusion control, both boride layers thicken at their common interface 2, as shown in Fig. 11. The FeB layer grows at the expense of diffusion of the B atoms across its bulk and their subsequent reaction with the Fe_2B compound. As a result, its thickness increases during dt by dx_{B_2}. The Fe_2B layer grows at the expense of diffusion of the Fe atoms across its bulk and their further reaction with the FeB compound. During the same time dt, its thickness increases by dy_{Fe_2}. Since the FeB and Fe_2B compounds are consumed in the formation

Table 2 Average Fe, Cr and B contents of reacting phases, found by EPMA measurements on X-ray diffraction samples (see Figs. 3, 6–8)

		Content (mass%/at-%)			
Section in Fig. 3	Region	Fe	Cr	B	Phase
I	One phase	71·7/42·6	12·1/7·7	16·2/49·7	(Fe,Cr)B
II	Darker in Fig. 6	70·7/41·7	12·8/8·1	16·5/50·2	(Fe,Cr)B
	Brighter in Fig. 6	77·8/56·4	13·3/10·3	8·9/33·3	(Fe,Cr)$_2$B
IV	One phase	76·9/55·9	14·3/11·1	8·8/33·0	(Fe,Cr)$_2$B
V	A in Fig. 7	78·8/57·9	12·8/10·1	8·4/32·0	(Fe,Cr)$_2$B
	B in Fig. 7	88·1/87·3	11·9/12·7	0·0/0·0	<Fe>
	C in Fig. 7	46·9/35·9	44·3/31·6	8·8/32·5	(Fe,Cr)$_2$B
VI	B in Fig. 8	87·4/85·9	12·4/13·1	0·0/0·0	<Fe>
	C in Fig. 8	54·5/38·6	36·3/27·7	9·2/33·7	(Fe,Cr)$_2$B
VII	One phase	85·2/84·3	14·8/15·7	0·0/0·0	<Fe>

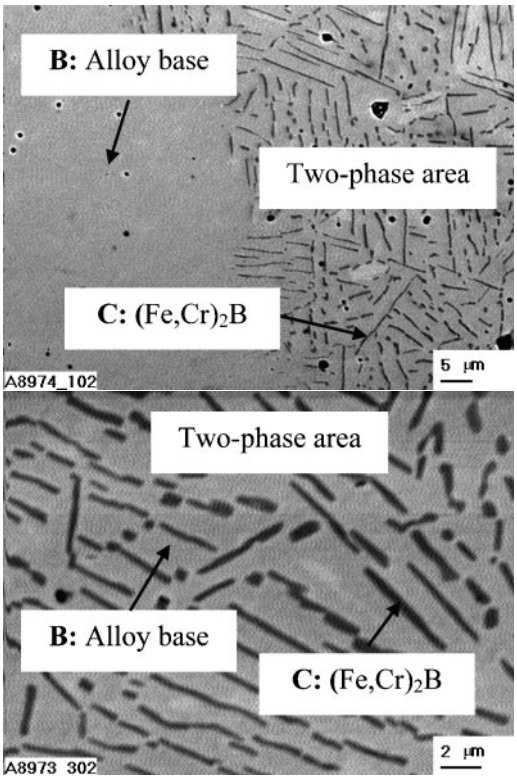

8 **Plan view micrographs corresponding to section VI in Fig. 3**

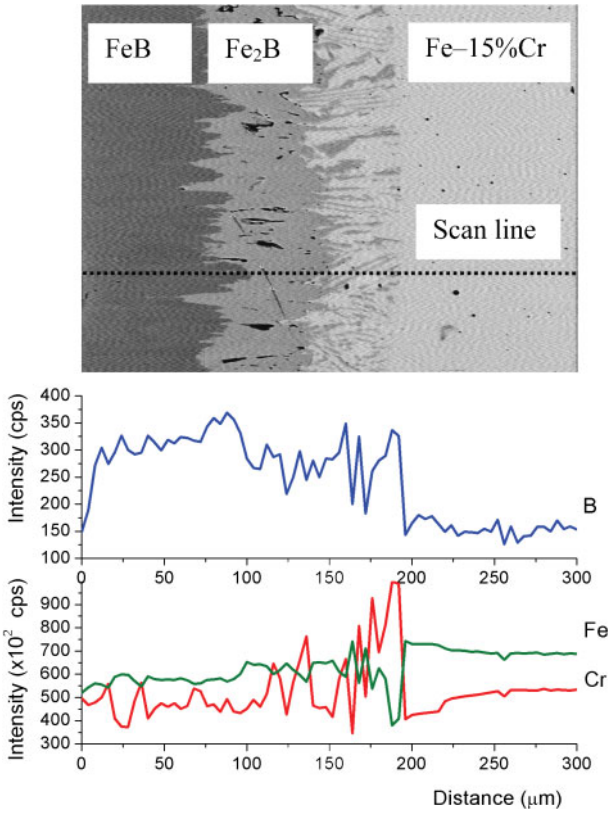

9 **Microstructure of transition zone between Fe–15Cr alloy and B, and concentration profiles of B, Fe and Cr: boriding conditions, temperature at 950°C and reaction time of 21 600 s (6 h)**

of each other, the thickness of the FeB layer simultaneously decreases by dx_- while that of the Fe_2B layer by dy_-. The net change of the FeB layer thickness during dt is the difference between dx_{B_2} and dx_-, while that of the Fe_2B layer thickness is the difference between dy_{Fe_2} and dy_-. Therefore, equations (2a) and (2b) contain two terms on their right hand parts.

Even though both boride layers are often considered to grow at the expense of diffusion of the single component B across their bulks, it is hardly possible with compact layers having no macroscopic defects (cracks, holes, fissures, etc.) and therefore growing by the volume diffusion mechanism. During diffusional growth, by definition, diffusion across the layer bulks is the rate determining step, the interface reactions being very fast. It means that all the B atoms reaching interface 2 react with Fe_2B to form FeB at that interface. Since, under conditions of diffusion control, the ability of interface 2 to combine those atoms exceeds their diffusional transport across the FeB layer (slow diffusion followed by fast reaction), none of them can diffuse

Table 3 Data (EPMA) for Fe–15Cr alloy–B diffusion zone formed after boriding at a temperature of 950°C for 21 600 s (6 h)

Material	Place of measurement	Content (mass%/at-%)			Phase
		Fe	Cr	B	
	At distance *l* away from the alloy/boride layer interface, μm				
Fe–Cr	–200	85·3/84·4	14·7/15·6	0·0/0·0	<Fe>
	–120	84·7/83·7	15·3/16·3	0·0/0·0	
	–60	86·1/85·2	13·9/14·8	0·0/0·0	
	–40	88·1/87·4	11·9/12·6	0·0/0·0	
	–20	86·3/85·4	13·6/14·5	0·02/0·11	
Inner boride layer	10	71·8/51·5	19·0/14·6	9·2/33·9	$(Fe,Cr)_2B$
	20	80·0/57·4	10·8/8·4	9·2/34·2	
	30	78·2/56·5	12·8/9·9	9·0/33·6	
	40	77·8/56·9	13·7/10·8	8·5/32·3	
	50	75·5/54·7	15·7/12·3	8·8/33·0	
	60	77·8/57·7	14·1/11·3	8·1/31·0	
Outer boride layer	70	71·2/42·6	12·8/8·2	16·0/49·2	(Fe,Cr)B
	80	71·3/42·0	12·2/7·8	16·5/50·2	
	90	70·5/41·6	13·0/8·2	16·5/50·2	
	100	71·7/43·0	12·5/8·0	15·9/49·0	
	110	71·6/42·3	12·0/7·6	16·4/50·1	

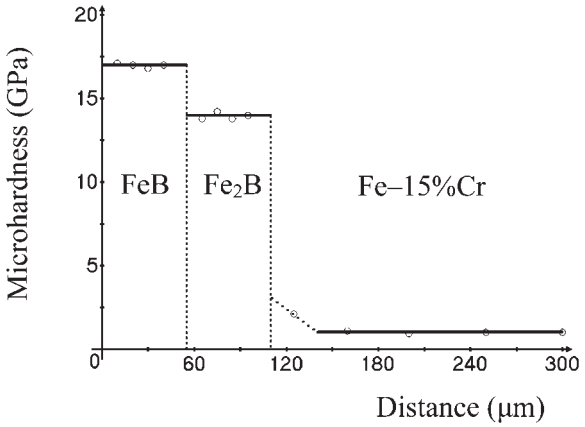

10 Plot of microhardness against distance within reacting phases: boriding conditions, temperature at 950°C and reaction time of 21 600 s (6 h)

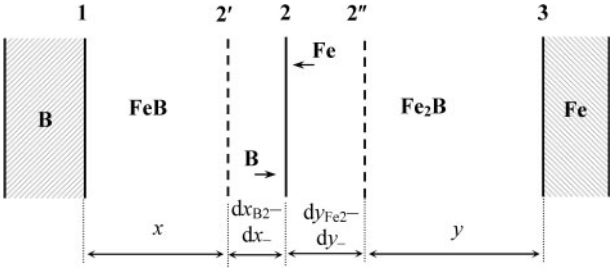

11 Schematic diagram to illustrate growth process of two boride layers under conditions of diffusion control. Both layers thicken at their common interface 2. No reactions take place at interfaces 1 and 3 in view of lack of appropriate diffusing atoms

further to interface 3 and react with Fe to form Fe_2B: $B_{dif}+2Fe=Fe_2B$.

This reaction can only take place either under conditions of reaction control when the flux of B atoms from the initial B containing phase is sufficient for both boride layers to grow (for more detail, see Ref. 39) or if the FeB layer is non-protective due to the presence of macroscopic defects. Reaction controlled growth is only typical of thin compound layers (<1 μm thick). The FeB layer was compact and therefore non-permeable to BF_3 and other gases. Hence, neither of these growth mechanisms could be operative with the boride layers investigated.

From a chemical viewpoint, it must thus be clear that the diffusionally growing FeB layer itself can, by no means, be a source of B atoms for the Fe_2B layer to grow. Suppose that two FeB molecules decompose at interface 2 to yield one molecule of Fe_2B and one diffusing B atom: $2FeB=Fe_2B+B_{dif}$. However, this B atom will be unable to diffuse from interface 2 to 3 because under conditions of diffusion control, the Fe_2B surface is undersaturated with B atoms; therefore, it is immediately combined at interface 2 according to the reaction $B_{dif}+Fe_2B=2FeB$. The net result of those reactions is seen to be zero. On the contrary, under conditions of reaction control, the Fe_2B surface bordering the FeB layer is oversaturated with B atoms, and therefore, a part of them (not combined into the FeB phase at interface 2) readily diffuses further to interface 3 and react with Fe atoms to form Fe_2B. As the only source of B atoms for both layers to grow is the boriding mixture (B and KBF_4), it is clear that, sooner or later, the flux of B atoms, diminishing as the FeB layer thickens, becomes only sufficient for the FeB layer itself to grow, whereas the faraway Fe_2B layer must stop growing.

Table 4 Thickness and kinetic constants for FeB and Fe_2B layers formed at Fe–15Cr alloy/B interface

Temperature, °C	Time, $\times10^2$ s	Thickness, $\times10^{-6}$ m			k_1 (from equation $x^2=2k_1t$), $\times10^{-14}$ m^2 s^{-1}			k (from system of equation (2)), $\times10^{-14}$ m^2 s^{-1}	
		Total	FeB	Fe_2B	Total	FeB	Fe_2B	k_B	k_{Fe}
850	36	31	15	16	13·3	3·1	3·6	18·4	25·0
	72	44	21	23	13·4	3·1	3·7	16·3	24·4
	108	55	25	30	14·0	2·9	4·2	8·58	12·3
	144	60	28	32	12·5	2·7	3·6	9·45	12·1
	180	70	33	37	13·6	3·0	3·8	10·8	14·1
	216	75	35	40	13·0	2·8	3·7	5·81	8·29
	252	80	36	44	12·7	2·6	3·8	8·57	9·30
	288	85	43	42	12·5	3·2	3·1	12·8	10·7
	360	95	50	45	12·5	3·5	2·8		
900	36	40	18	22	22·2	4·5	6·7	22·0	30·6
	54	50	23	27	23·1	4·9	6·8	12·5	14·4
	72	54	26	28	20·3	5·1	5·4	14·5	15·7
	90	65	31	34	23·5	5·3	6·4	17·0	21·2
	144	75	35	40	19·5	4·3	5·6	13·8	19·2
	180	85	40	45	20·1	4·4	5·6	16·0	19·7
	216	95	45	50	20·9	4·7	5·8	10·5	12·4
	288	100	47	53	17·4	3·8	5·2	10·9	13·2
	324	110	52	58	18·7	4·2	5·2		
950	36	55	23	27	34·7	7·3	10·1	50·3	75·2
	54	65	30	35	39·1	8·3	11·3	24·4	32·9
	72	70	32	38	34·0	7·1	10·0	14·2	19·2
	90	80	35	45	35·6	6·8	11·3	21·1	30·7
	108	90	39	51	37·5	7·0	12·0	17·0	24·2
	144	95	42	53	31·3	6·1	9·7	19·1	26·6
	180	110	50	60	33·6	7·0	10·0	25·9	33·7
	216	120	55	65	33·3	7·0	9·8	29·7	35·9
	252	140	65	75	38·9	8·4	11·2		

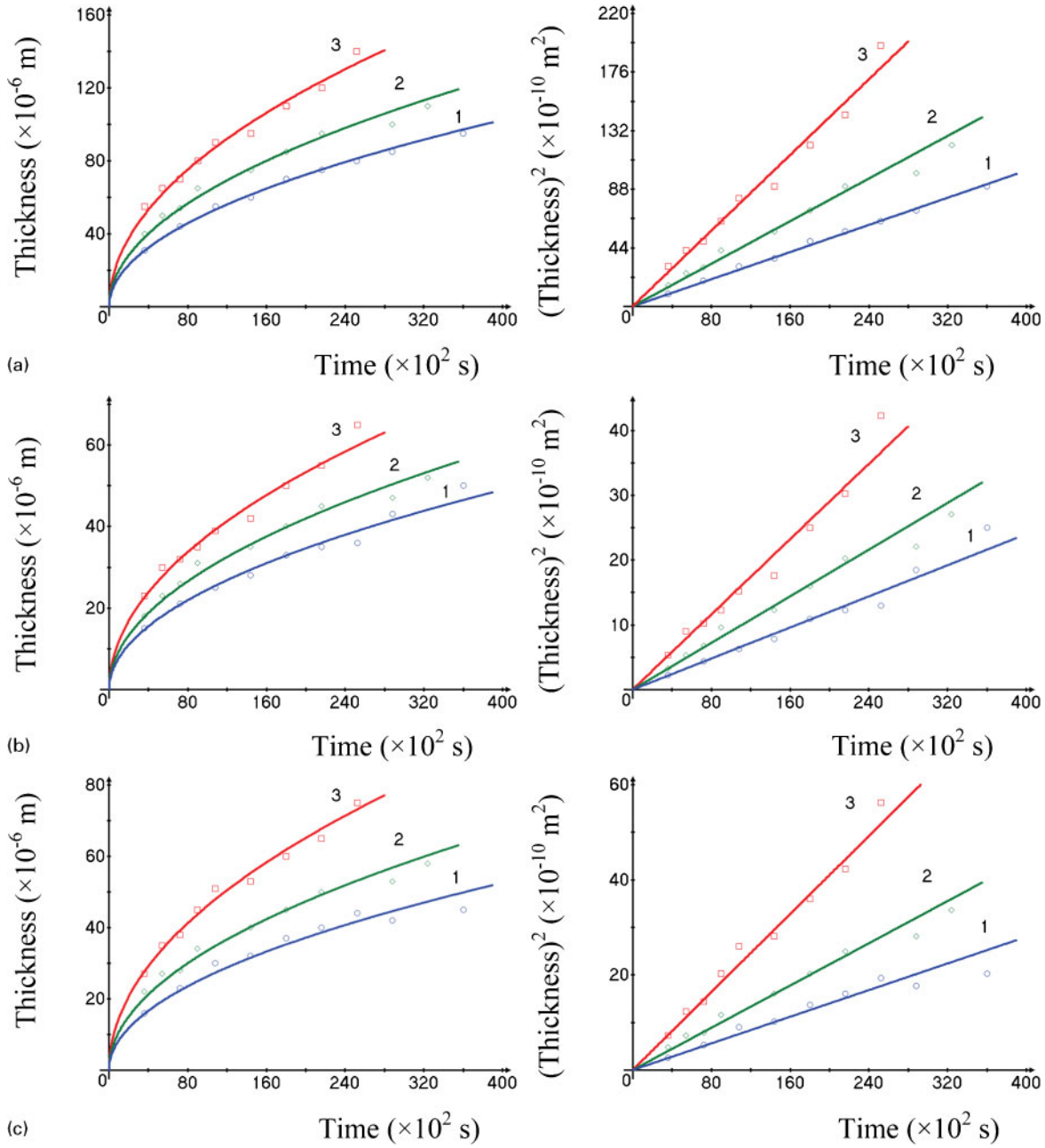

12 Plots of layer thickness (left) and squared layer thickness (right) against time for *a* both boride layers, *b* FeB layer and *c* Fe_2B layer formed between Fe–15Cr alloy and B at temperature of 850°C (line 1), 900°C (line 2) and 950°C (line 3)

Similarly, all the Fe atoms diffusing across the Fe_2B layer are combined into Fe_2B by their reaction with FeB at interface 2. Hence, Fe atoms cannot take part in the formation of the FeB layer at interface 1. Thus, under conditions of diffusion control, both boride (and any other compound) layers only grow at their common interface by pushing each other in opposite directions.

This conclusion is usually overlooked if the process of formation of compound layers is treated without writing the equations of chemical reactions proceeding at the layer interfaces. In fact, at the diffusional stage of layer formation, each of the two compound layers without any macroscopic defects can grow only at the expense of diffusion of the atoms of a neighbouring initial phase.

Even though grain boundary diffusion might also contribute to the layer growth process, its contribution appears to be much less compared to that of volume diffusion in view of the coarse grained structure of both layers. Therefore, in spite of the considerable difference in values of grain boundary diffusion and volume diffusion coefficients, the flux of diffusing atoms along grain boundaries could hardly be large.

An obvious criterion for the applicability of the system of equation (2) is the constancy of k_B and k_{Fe} over a given range of time, as is the case with both boride layers (Table 4). The value of g necessary for calculations of k_B and k_{Fe} was estimated from the densities $\rho_1=6{\cdot}70\times10^3$ kg m^{-3} and $\rho_2=7{\cdot}34\times10^3$ kg m^{-3} of the FeB and Fe_2B compounds[1] and their molecular masses $M_1=66{\cdot}65$ g mol^{-1} and $M_2=122{\cdot}49$ g mol^{-1}: $g=M_1\rho_2/M_2\rho_1=0{\cdot}60$.

The derivatives were found from the experimental layer thickness–time dependences by the numerical three point method using a conventional computer program

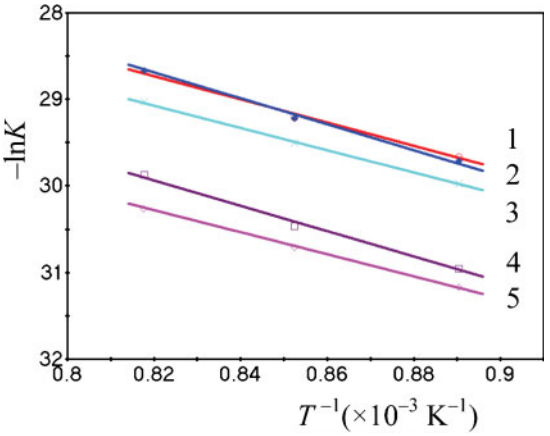

1: k_1 from equation $x^2=2k_1t$ for both boride layers; 2: k_{Fe} from system of equations (2); 3: k_B; 4: k_1 for Fe_2B; 5: k_1 for FeB

13 Temperature dependence of layer growth rate constants *K*

(linear approximation). To find a derivative for a given experimental point (x_i and t_i), like those on the left hand plots of Fig. 12, data for its two neighbouring points ($x_{i-1}$and t_{i-1}) and (x_{i+1} and t_{i+1}), including point $x_0=0$ at $t_0=0$, were used. Left and right hand derivatives $(x_i-x_{i-1})/(t_i-t_{i-1})$ and $(x_{i+1}-x_i)/(t_{i+1}-t_i)$, were first found for this point, and a mean value was then calculated. The derivatives could thus be found for all experimental points, excepting clearly the last one, for which a next neighbouring point is lacking.

As seen in Table 4, the results of calculations of k_B and k_{Fe} are strongly dependent upon a scatter of experimental points. To avoid this, approximation of experimental data with any suitable analytical function is therefore advisable. For example, the use of parabolic relations to approximate the layer thickness–time dependences and then to find the derivatives yields another set of values of k_B and k_{Fe} (Table 5). Since the experimental $x-t$ dependences become smoothed as a result of this procedure (solid lines on left hand plots of Fig. 12), all values of k_B thus found are identical. The same applies to k_{Fe}. Comparing these with the average values of k_B and k_{Fe} found numerically from the experimental points, it may be concluded that both sets of the constants agree fairly well (within $\pm10\%$), providing evidence for the validity of the analytical treatment employed. It is clear that, in order to obtain acceptable results, the optimum number of experimental points must be nine or more. With five or six points, calculations become problematic in view of a large computational uncertainty. Three or four points appear to be sufficient only for a preliminary estimation.

Note that the growth rate constants k_B and k_{Fe} are identified with the reaction diffusion coefficients of appropriate elements in boride layers (for more detail, see Ref. 39). The relative error of their determination is around $\pm15\%$. The main contribution to this value comes from an uncertainty in the determination of position of the interface between the growing boride layers due to their ragged morphology. It is worth mentioning, however, that the present case is not a worse one because the layer thickness was the same over the whole interface. In contrast, with many Fe based alloys and steels, island-like layers occur,[1] especially at a short time of boriding, which practically excludes any kinetic treatment.

As seen in Fig. 13, the temperature dependence of the layer growth rate constants is described in the 850–950°C range by a relation of the Arrhenius type

$$K=K_0\exp(-E/RT) \tag{3}$$

where K stands for any layer growth rate constant, E is the activation energy, R is the gas constant and T is the absolute temperature.

The least squares fit method yields the following equations:

$$k_1=1.95\times10^{-9}\exp(-103.8\text{ kJ mol}^{-1}/RT)\text{ m}^2\text{ s}^{-1}$$

for the FeB layer;

$$k_1=1.88\times10^{-8}\exp(-123.1\text{ kJ mol}^{-1}/RT)\text{ m}^2\text{ s}^{-1}$$

for the Fe_2B layer;

$$k_1=2.32\times10^{-8}\exp(-113.0\text{ kJ mol}^{-1}/RT)\text{ m}^2\text{ s}^{-1}$$

for both boride layers;

$$k_B=1{\cdot}00\times10^{-8}\exp(-107{\cdot}9\text{ kJ mol}^{-1}/RT)\text{ m}^2\text{ s}^{-1};$$

$$k_{Fe}=4{\cdot}38\times10^{-8}\exp(-119{\cdot}4\text{ kJ mol}^{-1}/RT)\text{ m}^2\text{ s}^{-1}.$$

Table 5 Average values of growth rate constants for FeB and Fe_2B layers formed at Fe–15Cr alloy/B interface

	k_1 (from equation $x^2=2k_1t$), $\times10^{-14}$ m^2 s^{-1}			k (from experimental points), $\times10^{-14}$ m^2 s^{-1}		k (from approximated dependences), $\times10^{-14}$ m^2 s^{-1}	
Temperature, °C	Total	FeB	Fe_2B	k_B	k_{Fe}	k_B	k_{Fe}
850	13·1±0·8	2·9±0·5	3·6±0·6	11·3	14·5	9·64	12·5
900	20·6±1·9	4·6±0·7	5·9±0·9	14·7	18·3	15·4	20·4
950	35·3±3·8	7·2±0·9	10·6±1·5	22·4	30·9	24·8	35·6

Table 6 Comparison of wear resistance of Fe–Cr alloy samples borided at 950°C for 21 600 s (6 h)*

Alloy	Δm_{base}, g	Δh_{base}, mm	r_1	$\Delta m_{boride\ layer}$, g	$\Delta h_{boride\ layer}$, mm	r_2	r_3
Fe–10Cr	0·32130	0·43	1·00	0·02875	0·035	11·2	1·00
Fe–15Cr	0·31060	0·41	1·03	0·00695	0·010	44·7	4·14
Fe–25Cr	0·29910	0·38	1·07	0·00095	~0·003	314·8	30·3

*Δm and Δh are changes in mass and height respectively of samples; $r_1=\Delta m_{base\ of\ a\ 10\%Cr\ alloy}/\Delta m_{base\ of\ a\ given\ alloy}$, $r_2=\Delta m_{base\ of\ a\ given\ alloy}/\Delta m_{boride\ layer\ on\ a\ given\ alloy}$, $r_3=\Delta m_{boride\ layer\ on\ a\ 10\%Cr\ alloy}/\Delta m_{boride\ layer\ on\ a\ given\ alloy}$.

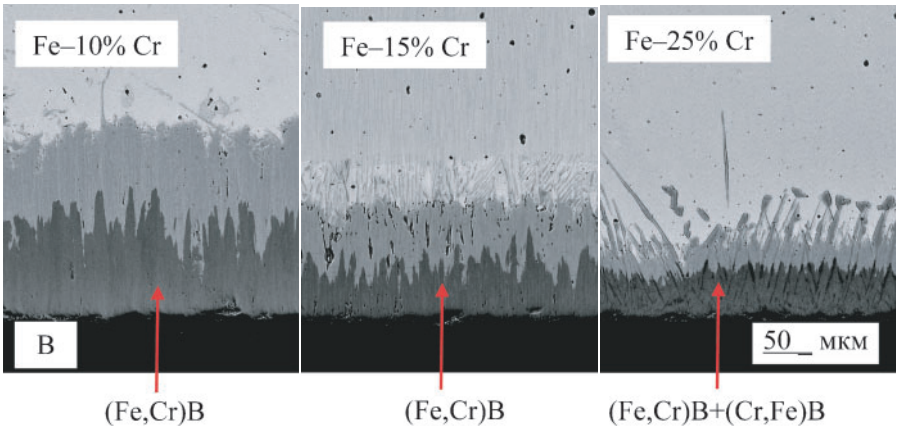

14 Backscattered electron images of Fe–Cr alloy/B interface: boriding conditions, temperature at 950°C and reaction time of 21 600 s (6 h)

Abrasive wear resistance of boride layers

Boriding the Fe–15Cr alloy tablets for dry abrasive wear resistance tests was carried out at 950°C for 6 h, producing the (Fe,Cr)B and $(Fe,Cr)_2B$ layers of thickness 55 and 65 μm respectively (120 μm in total). The wear resistance of any borided alloy sample, found from mass loss measurements, is around 45 times greater than that of the alloy base.

A comparison of the wear resistance of borided Fe–15Cr alloy samples with that of borided Fe–10Cr and Fe–25Cr alloy samples investigated earlier[40] is provided in Table 6. The wear resistance of the borided samples is seen to increase very significantly with increasing Cr content of the Fe–Cr alloys.

It is also easy to notice that the increase in wear resistance (around 30 times) of the Fe–Cr alloys investigated is non-proportional to the increase in their Cr content (2·5 times). Therefore, the main contribution to the increase in wear resistance of borided Fe–Cr alloys appears to come from the microstructure of boride layers (Fig. 14).

With Fe–10Cr and Fe–15Cr alloys, the outer boride layer consists of the homogeneous (Fe,Cr)B phase. In the case of a Fe–25Cr alloy; however, it consists of the platelets of the (Fe,Cr)B and (Cr,Fe)B phases, located at an angle of around 45° to each other. These platelets thus form a rigid framework of enhanced wear resistance. The same applies to the inner boride layer.

Conclusions

1. Two boride phases (Fe,Cr)B and $(Fe,Cr)_2B$ occur as separate layers at the interface between a Fe–15Cr alloy and B at 850–950°C and reaction times up to 12 h. The Cr content is 8 ± 1 at-% in the outer (Fe,Cr)B layer and 12 ± 2 at-% in the inner $(Fe,Cr)_2B$ layer.

2. The characteristic feature of both layers is a pronounced texture, the strongest reflections being {002} and {020} for the orthorhombic FeB phase and {002} for the tetragonal Fe_2B phase.

3. Diffusional growth kinetics of the boride layers are close to parabolic and can alternatively be described by a system of two non-linear differential equations. Both approaches yield a good fit to the experimental data.

4. Microhardness values are $17{\cdot}4\pm0{\cdot}9$ GPa for the (Fe,Cr)B layer, $14{\cdot}4\pm0{\cdot}8$ for the $(Fe,Cr)_2B$ layer and $0{\cdot}95\pm0{\cdot}08$ GPa for the Fe–15Cr alloy base.

5. The dry abrasive wear resistance of borided Fe–15Cr alloy samples is ~45 times greater than that of the alloy base.

References

1. L. G. Voroshnin and L. S. Lyakhovich: 'Borirovaniye stali'; 1978, Moscow, Metallurgiya.
2. A. G. Matuschka: 'Boronizing'; 1980, Munchen, Carl Hanser Verlag.
3. L. G. Voroshnin: 'Borirovaniye promyshlennikh staley i chugunov'; 1981, Minsk, Belarus.
4. A. K. Sinha: 'Boriding (boronizing)', in 'Metals handbook', (ed. A. K. Sinha), 844; 1982, Metals Park, OH, ASM International.
5. H. Kunst, H. Schroll, R. Luetje, K. Wittel, E. Lugscheider, T. Weber, H. R. Eschnauer and C. Raub: 'Metals, surface treatment', 'Ullmann's encyclopedia of industrial chemistry', Vol. A16, 427; 1991, Weinheim, Verlag Chemie.
6. E. Takeuchi, K. Fujii and T. Katagiri: 'Sliding wear characteristics of gas boronized steel', *Wear*, 1979, **55**, (1), 121–130.
7. M. Carbucicchio, L. Bardani and G. Palombarini: 'Mössbauer and metallographic analysis of borided surface layers on Armco iron', *J. Mater. Sci.*, 1980, **15**, (3), 711–719.
8. K.-H. Habig and R. Chatterjee-Fischer: 'Wear behaviour of boride layers on alloyed steels', *Tribol. Int.*, 1981, **14**, (4), 209–215.
9. P. Goeuriot, R. Fillit, F. Thevenot, J. H. Driver and H. Bruyas: 'The influence of alloying element additions on the boriding of steels', *Mater. Sci. Eng.*, 1982, **55**, (1), 9–19.
10. P. Goeuriot, F. Thévenot, J. H. Driver and T. Magnin: 'Methods for examining brittle layers obtained by a boriding surface treatment (Borudif)', *Wear*, 1983, **86**, (1), 1–10.
11. G. Palombarini, M. Carbucicchio and L. Cento: 'Electron probe microanalysis of nickel and chromium in Fe–Cr–Ni and Fe–C–Cr alloys borided at 850°C', *J. Mater. Sci.*, 1984, **19**, (11), 3732–3738.
12. M. Carbucicchio and G. Sambogna: 'Influence of chromium on boride coatings produced on iron alloys', *Thin Solid Films*, 1985, **126**, (3–4), 299–305.
13. M. Carbucicchio and G. Palombarini: 'Effects of alloying elements on the growth of iron boride coatings', *J. Mater. Sci. Lett.*, 1987, **6**, (10), 1147–1149.
14. C. M. Brakman, A. W. J. Gommers and E. I. Mittemeijer: 'Boriding of Fe and Fe–C, Fe–Cr and Fe–Ni Alloys. Boride-layer growth kinetics', *J. Mater. Res.*, 1989, **4**, (6), 1354–1370.
15. K. Genel, I. Ozbek and C. Bindal: 'Kinetics of boriding of AISI W1 steel', *Mater. Sci. Eng. A*, 2003, **A347**, (1–2), 311–314.
16. I. Campos, J. Oseguera, U. Figueroa, J. A. García, O. Bautista and G. Kelemenis: 'Kinetic study of boron diffusion in the paste-boriding process', *Mater. Sci. Eng. A*, 2003, **A352**, (1–2), 261–265.
17. M. Kulka and P. Pertek: 'Microstructure and properties of borided 41Cr4 steel after laser surface modification with re-melting', *Appl. Surf. Sci.*, 2003, **214**, 278–288.

18. C. Martini, G. Palombarini and M. Carbucicchio: 'Mechanism of thermochemical growth of iron borides on iron', *J. Mater. Sci.*, 2004, **39**, (3), 933–937.
19. C. Martini, G. Palombarini, G. Poli and D. Prandstraller: 'Sliding and abrasive behaviour of boride coatings', *Wear*, 2004, **256**, 608–613.
20. A. A. Novakova, I. G. Sizov, D. S. Golubok, T. Yu. Kiseleva and P. O. Revokatov: 'Electron-beam boriding of low-carbon steel', *J. Alloys Compd*, 2004, **383**, (1–2), 108–112.
21. E. Galvanetto, F. Borgioli, T. Bacci and G. Pradelli: 'Wear behaviour of iron boride coatings produced by VPS technique on carbon steels', *Wear*, 2006, **260**, (7–8), 825–831.
22. S. Taktak: 'A study on the diffusion kinetics of borides on boronized Cr-based steels', *J. Mater. Sci.*, 2006, **41**, (22), 7590–7596.
23. I. Campos, R. Rosas, U. Figuero, C. VillaVelázquez, A. Meneses and A. Guevara: 'Fracture toughness evaluation using Palmqvist crack models on AISI 1045 borided steels', *Mater. Sci. Eng. A*, 2008, **A488**, (1–2), 562–568.
24. X. Tian, Y. Lu, S. J. Sun, Z. G. Wang, W. Q. Hao, X. D. Zhu and Y. L. Yang: 'Effect of boronising on mechanical properties, wear and corrosion of N80 steel', *Mater. Sci. Tech.*, 2008, **24**, (3), 314–319.
25. M. Hansen: 'Constitution of binary alloys', 2nd edn; 1958, New York, McGraw-Hill.
26. H. Okamoto: 'B–Fe (boron–iron)', *J. Phase Equilib. Diff.*, 2004, **25**, 297–298.
27. V. I. Dybkov, W. Lengauer and K. Barmak: 'Formation of boride layers at the Fe–10%Cr alloy–boron interface', *J. Alloys Compd*, 2005, **398**, (1–2), 113–122.
28. J. Brandstötter and W. Lengauer: 'Multiphase reaction diffusion in transition metal-boron systems', *J. Alloys Compd*, 1997, **262–263**, 390–396.
29. V. I. Dybkov, W. Lengauer and K. Barmak: 'Abrasive wear resistance of pack-borided iron–chromium alloys', Proc. 16th Plansee Seminar, Reutte, Austria, Carl Hanser Verlag, May–June 2005, 999–1009.
30. L. I. Mirkin: 'Spravochnik po rentgenostructurnomu analizu polokristallov'; 1961, Moscow, Fizmatgiz.
31. S. S. Gorelik, L. N. Rastorguev and Yu. A. Skakov: 'Rentgenograficheskiy i electronno-opticheskiy analiz: prilozheniya'; 1970, Moscow, Metallurgiya.
32. V. A. Barinov, G. A. Dorofeev, L. V. Ovechkin, E. P. Elsukov and A. E. Ermakov: 'Structure and magnetic properties of the α-FeB phase obtained by mechanical working', *Phys. Status Solidi A*, 1991, **123A**, 527–534.
33. C. Gianoglio and C. Badini: 'Distribution equilibria of iron and nickel in two phase fields of the Fe–Ni–B system', *J. Mater. Sci.*, 1986, **21**, 4331–4334.
34. S. Okada, T. Atoda and I. Higashi: 'Structural investigation of Cr_2B_3, Cr_3B_4, and CrB by single-crystal diffractometry', *J. Solid State Chem.*, 1987, **68**, 61–67.
35. C. Gianoglio, G. Pradelli and M. Vallino: 'Solid state equilibria in the Cr–Fe–B system at the temperature of 1373 K', *Metall. Sci. Technol.*, 1983, **1**, 51–57.
36. A. Bondar: 'Boron–chromium–iron', in 'Landolt–Börnstein, numerical data and functional relationships in science and technology, (New Series) Group IV: physical chemistry', (ed. W. Martinsen), 'Ternary alloy systems. Phase diagrams, crystallographic and thermodynamic data critically evaluated by MSIT', (ed. G. Effenberg and S. Ilyenko), Vol. 11D1, 320–343; 2007, Berlin/Heidelberg, Springer.
37. W. Seith: 'Diffusion in metallen'; 1955, Berlin, Springer.
38. K. Hauffe: 'Reaktionen in und an festen Stoffen'; 1955, Berlin, Springer.
39. V. I. Dybkov: 'Reaction diffusion and solid state chemical kinetics'; 2002, Kyiv, The IPMS Publications.
40. V. I. Dybkov, L. V. Goncharuk, V. G. Khoruzha, K. A. Meleshevich, A. V. Samelyuk and V. R. Sidorko: 'Growth kinetics of boride layers on iron–chromium alloys and their dry abrasive wear resistance', in Proc. Conf. on 'Materials science and technology' (MS&T-2007): 'Fundamentals and characterization: phase stability, diffusion and their applications', Detroit, MI, USA, September 2007, American Ceramic Society, 513–524.